ELSEVIER

Neurobiology of Aging 27 (2006) 835–847

NEUROBIOLOGY OF AGING

www.elsevier.com/locate/neuaging

In vivo MRI and histological evaluation of brain atrophy in APP/PS1 transgenic mice

Benoît Delatour [a], Maryvonne Guégan [a], Andreas Volk [b], Marc Dhenain [b,*]

[a] *Laboratoire NAMC, CNRS, UMR 8620, Bât 446, Université Paris Sud, 91405 Orsay, France*
[b] *Curie Institute, U350 INSERM, Centre Universitaire, Laboratoire 112, 91405 Orsay Cedex, France*

Received 6 November 2004; received in revised form 6 April 2005; accepted 26 April 2005
Available online 14 July 2005

Abstract

Regional cerebral atrophy was evaluated in APP/PS1 mice harboring mutated transgenes linked to familial Alzheimer's disease, using complementary methods. In vivo high resolution MRI was selected for measurements of brain atrophy and associated cerebrospinal fluid dilation; histological analysis was performed to reveal localized atrophies and to evaluate amyloid burden.

Young APP/PS1 mice examined at a pre-amyloid stage (10 weeks) showed disruption in development (reduced intracranial and brain volumes). Comparison of young and old (24 months) mice, indicated that both APP/PS1 and control brains endure growth during adulthood. Aged APP/PS1 animals showed a moderate although significant global brain atrophy and a dilation of CSF space in posterior brain regions. The locus of this atrophy was identified in the midbrain area and not, as expected, at isocortical/hippocampal levels. Atrophy was also detected in fiber tracts. The severity of brain atrophy in old APP/PS1 mice was not correlated with the extent of cerebral amyloidosis. The relevance of current transgenic mouse models for the study of brain atrophy related to Alzheimer's disease is discussed.

Keywords: Alzheimer's disease; APP; Amyloid precursor protein; Aβ peptide; Atrophy; Brain; MRI; PS1; Presenilin; Mouse; Animal model; Transgenesis; Midbrain; Fiber tracts; Morphometry; Hippocampus; Development

1. Introduction

Neuropathological hallmarks of Alzheimer's disease (AD) are senile plaques and neurofibrillary tangles (NFT). These lesions are mostly distributed in isocortical and hippocampal brain areas. Senile plaques are extracellular deposits of amyloid-β (Aβ) peptides surrounded by dystrophic neurites while tangles are pathological filaments primarily located in neuronal cell bodies and made of hyperphosphorylated tau proteins [20].

At the macroscopic level, brains from AD patients are characterized by a severe atrophy leading to dilation of the ventricular system and a widening of cortical sulci [43]. However, atrophy in AD is not a homogeneous process and, in the early stages of the disease, it affects mainly medial temporal areas including the hippocampal formation [22]. Atrophy of these regions has been repeatedly reported to correlate with local density of NFT [3,25]. Progression of neurofibrillary lesions across isocortical areas (according to Braak and Braak stages [5]) has also been described as a good predictor of medial temporal lobe atrophy [18,24]. These observations suggest that NFT accumulation is crucially involved in the atrophy process [3,25], at least in the medial temporal areas that are the first regions to display neurofibrillary alterations in the early stages of the disease [5].

A relationship, although low, has been described between amyloid load and atrophy of the temporal lobe [25]. This suggests that Aβ deposition per se is also involved in the atrophy process even if its role, in AD patients, is underscored by the predominant deleterious incidence of neurofibrillary lesions. In any case, because of the simultaneous occurrence of both amyloid and neurofibrillary alterations in humans, it remains difficult to decipher how each of these primary neuropathological lesions participates in the genesis of cerebral atrophy in AD patients.

* Corresponding author. Tel.: +33 1 69 86 31 64; fax: +33 1 69 07 53 27.
E-mail address: Marc.Dhenain@curie.u-psud.fr (M. Dhenain).

0197-4580/$ – see front matter © 2005 Elsevier Inc. All rights reserved.
doi:10.1016/j.neurobiolaging.2005.04.011

Answering the question of the relationship between each AD lesion and brain atrophy could be facilitated using transgenic animal models mimicking specific AD-related neuropathological alterations (e.g., amyloid deposits without NFTs) and therefore being prone to develop brain atrophy associated with "isolated" microscopic lesions.

Many AD transgenic mouse models are based on the overexpression of human mutated genes (Aβ precursor protein (APP) and presenilin-1 (PS1)) associated with familial AD [17]. In the different lines that have been created up to now, neither NFT nor significant neuronal loss could be detected (e.g., [39]) except in one recently developed APP/PS1 knock-in model with localized neuronal loss in CA1/2 [7]. On the contrary, these mice are characterized by a graded age-related cerebral amyloidosis, associated with detrimental effects on the behavioral phenotype [1]. This supports the assumption that Aβ is a core lesion that induces a sequence of pathogenic events, resulting in increased levels of cerebral alterations and promoting behavioral disturbances [15]. One might therefore suspect, in accordance with this "amyloid cascade hypothesis" that transgenic mice overexpressing mutated APP should develop brain atrophy as a consequence of Aβ accumulation. Highlighting a relationship between brain atrophy and amyloid load might also be useful to screen the macroscopic effects of drugs and immunotherapies aimed at reducing or preventing the amyloid deposition [12].

Several studies have been carried out to determine the occurrence of selective brain atrophies in one transgenic mouse line (PDAPP model) reproducing AD-like cerebral amyloidosis [11,14,32,45]. These investigations reported compelling evidence of atrophy of the hippocampus, fornix and corpus callosum. However, because of their early occurrence, these lesions might be viewed as being caused by a neurodevelopmental deficit rather than by age-related brain shrinkage induced by Aβ deposits. The lack of observations in other transgenic lines than the PDAPP model also weakens the contention that brain amyloidosis is invariably accompanied by cerebral atrophy.

The aim of the present study was therefore to: (1) characterize the pattern of cerebral atrophy in a new transgenic line expressing both human mutant APP and PS1. These mice have been recently characterized at the neuropathological level [2,46,47] and constitute a more aggressive model of cerebral amyloidosis than single APP transgenic lines. (2) Evaluate the relationship between cerebral atrophy and Aβ deposition (amyloid load) in this APP/PS1 line.

APP/PS1 mice were first studied at a young age (10 weeks), preceding cerebral amyloid deposition [2]. Double transgenics were also studied at 2 years of age when they show high amyloid load with extended number of aggregated mature plaques in numerous brain areas [2]. For all analyses, age-matched PS1 (amyloid free) mice were used as controls.

Several approaches were taken to evaluate brain atrophies. First, brain volumes were estimated by in vivo magnetic resonance imaging (MRI). This method, also used in two previous studies [32,45], prevents tissue distortion associated with brain removal, fixation and sectioning and is well suited for longitudinal studies. In the present study, global and regional cerebral atrophy were evaluated on in vivo MR images by directly measuring brain volume and also by evaluating cerebrospinal fluid (CSF) volumes in all ventricles and peri-encephalic areas [9,10]. The latter measurements were based on the fact that brain atrophy leads to an increase of CSF volume in the regions close to the atrophied tissue [10].

Brain atrophy was also studied, following brain extraction, by extrapolating global and regional morphological measurements from serial histological sections (see also [11,14,32]). These postmortem analyses were correlated with in vivo MRI measurements (see also [32]).

Finally, to better assess the relationship between brain atrophy and Aβ deposition in old APP/PS1 mice, the amyloid load of each animal was neuropathologically assessed and correlated with MRI- and histology-based brain morphometry.

2. Material and methods

2.1. Transgenic mice

Double Thy1 APP751 SL (Swedish mutation KM670/671NL, London mutation V717I introduced in the human APP751 sequence) × HMG PS1 M146L transgenic mouse line was generated and established in accordance with standard procedures using CBA/C57Bl6 hybrids [2,34,46]. APP/PS-1 double-transgenic mice were generated by crossing PS1 homozygous mice with hemizygous APP transgenic mice. In these double transgenic mice, the amyloid deposition starts at the age of 2.5 months [2,46,47]. The PS1 mice had been back-crossed on a C57Bl6 background for more than six generations, whereas the APP mice were on a CBA (12.5%) C57Bl6 (87.5%) background.

Female APP/PS1 mice were compared with age-matched, female, amyloid-free PS1 animals. Two age groups were evaluated: 10-week-old animals (eight APP/PS1 and seven PS1 mice) and 24-month-old mice (seven APP/PS1 and nine PS1). One aged APP/PS1 animal with abnormally large CSF volumes and two aged PS1 animals with brain tumors were discarded from statistical analyses.

2.2. MRI experiment

Brain images (Fig. 1A–C and G) were recorded on a 4.7 T Bruker Biospec 47/30 system, equipped with a 12-cm diameter gradient system (200 mT/m). A surface coil (diameter = 30 mm), actively decoupled from the transmitting birdcage probe (Bruker GmbH) was used for signal acquisition. Animals were anesthetized by isoflurane (5% for induction, 1–2% for maintenance). Respiration rate was monitored to insure animal survival until the end of the experiment.

Three-dimensional fast spin-echo (RARE) images were recorded with an isotropic nominal resolution of

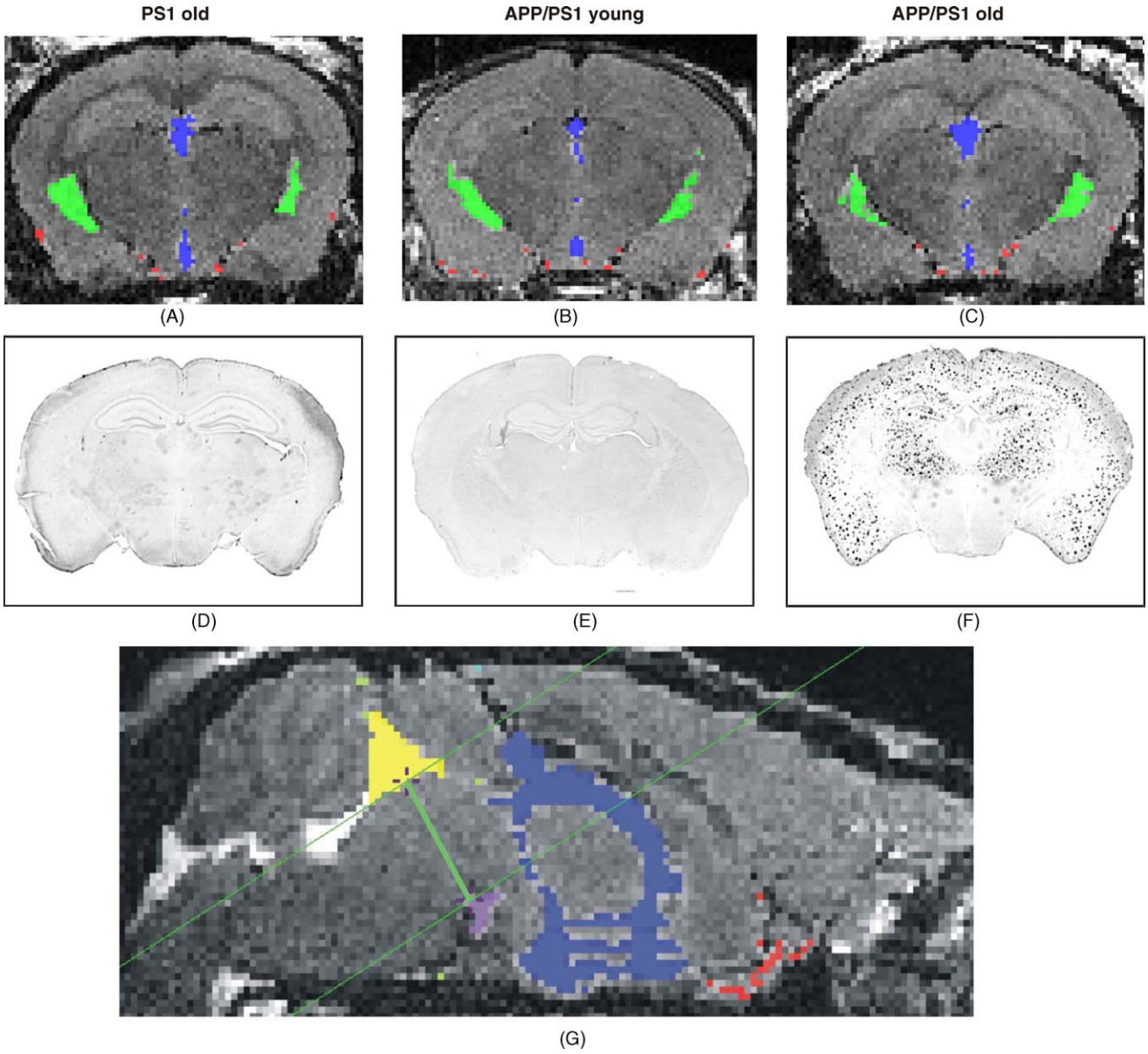

Fig. 1. MRI (A–C) and Congo red stained (D–F) coronal sections, at the level of the dorsal hippocampus, of APP/PS1 (B, C, E, F) and PS1 (A, D) animals. MRI sagittal view of the brain of an APP/PS1 animal is illustrated in panel (G). On MR sections CSF regions are labeled as follows: green, CSF_{LV}; blue, CSF_{3V}; red, CSF_{antC}; purple, CSF_{mam}; pale green, $CSF_{midbrain}$; yellow, CSF_{sylv}. The large green line in (G) represents the distance used to measure the height of the midbrain on MRI images; the thin green lines were taken as landmarks to evaluate this height between the basis of the aqueduct of Sylvius and the roof of the mammillary fossa. Note the high density of plaques in the aged APP/PS1 mouse (F) and the absence of amyloid Aβ deposition in the young mice of the same genotype (E) and in PS1 control animal (D). (For interpretation of the references to colour in this figure legend, the reader is referred to the web version of the article.)

117.2 μm (TR/TE/weighted-TE = 2500/10/75.4 ms, RARE factor = 16, NA = 1, field of view = 3 cm × 1.5 cm × 1.5 cm, matrix = 256 × 128 × 128). A "flip-back" was applied to enhance the signal from CSF [9]. The sensitivity gradient resulting from surface coil acquisition was corrected by a phantom based method as previously described [9]. Then, the MR brain images from the different mice were rotated to be positioned in similar orientation (code written under IDL 5.4).

2.3. Segmentation protocol

2.3.1. Intracranial volume assessment

The brain and surrounding CSF were semi-automatically extracted from other head tissue, by an observer blind to the animal genotype, using AMIRA software (Mercury Computer Systems Inc., TGS Unit, Villebon, France). First, a threshold was visually defined to automatically segment the brain and surrounding CSF from other brain tissues (label

voxel and remove island tools). This threshold was easy to find thanks to the high contrast between intracranial structures (brain and CSF) and other tissue. Then, this initial segmentation was manually refined (drawing tools) on a slice-by-slice basis. Borders were then smoothed (AMIRA smooth tool). The first and last slices corresponded, respectively, to the most anterior part of the frontal pole (including peri-encephalic CSF) and to the most posterior part of the occipital cortex (including peri-encephalic CSF). Brain sampling volume was therefore performed between +3.56 mm and −4.72 mm from Bregma [28]. The length of the antero-posterior axis of each brain was defined by counting the number of sections between these two slices and then by multiplying this number by 117.2 μm (MRI slice thickness). An average of 77 coronal sections were outlined for each animal. The surface of each section and then the global volume, referred to as the intracranial volume (V_{intC}), were evaluated (AMIRA tissue statistic tool).

2.3.2. Evaluation of CSF volumes

CSF volume was evaluated from the same MRI brain slices used to calculate the intracranial volume. The intensity threshold separating CSF pixels from other pixels was computed using the following method: The signal intensity (I) and its standard deviation (S.D.) were assessed in the amygdala. Pixels that displayed an intensity superior to $I + 4.41717 \times$ S.D. were considered to be CSF (4.41717 corresponds to a 0.001% confidence interval for a Gaussian population). CSF voxels were manually labeled and classified as belonging to various brain areas (see Fig. 1A–C and G) by using a freeware (display available at ftp.bic.mni.mcgill.ca) that allowed the control of voxel labeling in the three directions. The CSF areas were defined, as follows: first the brain was divided into its anterior and posterior parts, separated by the first slice displaying the interpeduncular fossa. CSF in the anterior part of the brain was classified into (1) CSF in the part of the lateral ventricle located posterior to the interventricular foramen (CSF_{LV}). This region of interest was selected because it is an area where the lateral ventricles surround the dorsal hippocampus. Its dilation might thus reflect hippocampal atrophy. (2) CSF in the third ventricle and in the part of the lateral ventricle anterior to the interventricular foramen (CSF_{3V}). (3) CSF in the anterior peri-encephalic areas (CSF_{antC}). CSF in the posterior part of the brain was classified into (1) CSF in the mammillary fossa (or interpeduncular fossa) (CSF_{mam}). (2) CSF located around the midbrain ($CSF_{midbrain}$). (3) CSF in the aqueduct of Sylvius (CSF_{sylv}). (4) CSF in other posterior peri-encephalic areas (CSF_{postC}). (5) Some voxels localized at the junction between the temporal and occipital areas were hyperintense because of susceptibility effects caused by the internal ears located just underneath this area. They were labeled as artifactual voxels. Their determination was made by a single user who was blind to the animal genotype. Once images from all animals had been labeled, we double-checked that the voxel attribution to the different regions was consistent for all animals. Then, the number of voxels belonging to each region was automatically counted by the 'Display' freeware. We controlled that the number of inner ear-related artifactual voxels did not differ between the four animal groups (U's > 9, ns).

A score of global brain atrophy was evaluated by summing up CSF volumes from all brain regions. To correct for inter-individual differences in skull size, the ratios between CSF volumes and intracranial volumes were computed on both total and regional (anterior or posterior) raw CSF data. These corrected measures were termed as "indices".

2.3.3. Direct evaluation of brain volume and of midbrain height

A direct MRI-based evaluation of brain volume (V_{Br}) was performed by removing the volume of CSF surrounding the brain from the intracranial volume:

$$V_{Br} = V_{intC} - (CSF_{antC} + CSF_{postC} + CSF_{mam} + CSF_{midbrain}) \quad (1)$$

To take into account differences in intracranial size, the ratio between V_{Br} and intracranial volume was calculated as a corrected measure of global brain atrophy (see also [32,45]).

Midbrain height was determined, on sagittal views of the brain, as the distance between the basis of the aqueduct of Sylvius and the roof of the mammillary fossa (Fig. 1G).

2.4. Neuropathology

Animals were rapidly decapited after imaging and their brain was fixed in 10% buffered formalin for 5–10 days. Brains were subsequently sectioned into 40 μm thick coronal sections on a freezing microtome. Sections ranged from the frontal pole to the end of the caudal part of the hippocampus. Obviously, the brain sampling volume used for histological material (approximately assessed from Bregma +3.20 mm to Bregma −4.04 mm according to Paxinos [28]) was smaller than that covered by the MRI measurement (see above).

One out of eight serial floating sections were rinsed with 0.1 M phosphate buffer and mounted on gelatine-coated glass slides before being processed for Nissl and Congo red staining [30]. Each slice was then digitized using a Super CoolScan 8000 ED high-resolution scanner (Nikon, Champigny sur Marne, France).

2.4.1. Evaluation of brain and hippocampal volumes

The brain volume and the volume of the hippocampi were assessed from Nissl and Congo red stained serial sections. Volumes were then estimated from serial surfaces according to an adapted Cavalieri method [33] and were normalized after calibration in Photoshop (Adobe, Paris, France) to be expressed in mm^3. A correction of the hippocampal volume was calculated by dividing the hippocampal volume by the brain volume. Some brain sections from one 24-month-old PS1 animal had been altered during histological processing.

Consequently, volumetric data (and also measurements of corpus callosum length; see below) from this animal were excluded from statistical analysis.

2.4.2. Evaluation of atrophy in selected brain structures (fiber tracts, mammillary bodies and midbrain area)

All morphological measures (distances or surfaces), with the exception of the corpus callosum length, were performed, following manual delineation on digitized histological sections, with the measure tools of Photoshop 6.

The antero-posterior length of corpus callosum was determined as the distance between the most rostral and caudal slices where it could be identified. Corpus callosum thickness was evaluated at two antero-posterior levels as the distance between its most ventral and dorsal points. Rostral thickness was measured on the first frontal slice where the corpus callosum could be identified (corresponding approximately to +1 mm/Bregma according to [28]). Caudal thickness was measured on the first slice where the dorsal hippocampus was present (corresponding approximately to −1 mm/Bregma [28]). The fornix diameter was measured at the same level as the caudal corpus callosum thickness. Diameter of the mammillothalamic tract was measured at −1.5 mm/Bregma [28]. This anatomical level was easily identified in all studied mice.

The surface of the mammillary bodies was evaluated at a stereotaxic level close to −2.7 mm/Bregma [28]. For one 24-month-old PS1 animal, clear delineation of the mammillary bodies at this stereotaxic level was impossible and therefore this mouse was not included in statistical analysis.

The surface of the internal capsule was measured at the level of rostral dorsal hippocampi (approximatively −1.06 mm/Bregma) that was easily identified in all animals, except one 24-month-old APP/PS1 mouse. The area of the internal capsule was manually redrawn from microscopic photographs.

Finally, the midbrain width was measured at −3.4 mm/Bregma [28]. The width of the midbrain was defined as the largest right–left distance of the structure. In all animals, this transverse diameter was perpendicular to the Sylvius aqueduct.

2.4.3. Evaluation of the amyloid load

Amyloid load was quantified on Congo red stained material (see Fig. 1F) using computer-based thresholding methods. Each stained section was binarized after thresholding in Photoshop. Binarized images were then transferred to Image-Pro Plus software (Media Cybernetics, Silver Spring, USA) and submitted to a particle-detection algorithm to count the number of plaques and measure their surface on each brain section. The proportion of tissue area occupied by Congo red stained material, which corresponds to the proportion of volume according to Delesse principle [8] was assessed from a total of 13–15 brain slices per animals. This ratio (surface stained/whole section surface) was taken as a global measure of the cerebral "amyloid load" of each individual mice.

Evaluation of the amyloid load was only performed on 24-month-old APP/PS1 mice as only a very few congo red positive deposits were observed in young double transgenics.

2.5. Statistical analysis and individual studies

Descriptive statistics were illustrated using means and standard errors to the mean (S.E.M.) of each age/genotype groups' values. Non-parametric Mann–Whitney's *U*-tests and linear correlations were used to compare the animal groups (Statistica 6; StatSoft Inc., Tulsa, USA).

3. Results

3.1. Global brain atrophy

Brain length assessed by MRI was similar in 10-week-old APP/PS1 and PS1 animals (Mann–Whitney's $U = 15.5$, ns). A significant increase of brain length occurred subsequently with aging in APP/PS1 mice ($U = 2$, $p < 0.005$) but not in PS1 animals ($U = 23$; ns). Accordingly brain length was significantly higher in 24-month-old APP/PS1 animals than in aged-matched PS1 mice ($U = 2$, $p < 0.005$).

A positive correlation was obtained between in vivo and postmortem measures of global, non-corrected, brain volumes ($r = 0.617$; $p < 0.001$). MRI assessment of brain volume was nevertheless considered to be more accurate than neuropathological evaluation. Therefore, statistical analysis of global brain volumes presented below were only performed using in vivo MRI measurements.

Evaluation of intracranial and non-corrected brain volumes in 10 weeks old animals revealed lower volumes in APP/PS1 than in PS1 animals (U's = 3, $p < 0.005$; see Fig. 2A). During aging both intracranial and brain volumes increased in APP/PS1 mice (U's < 5, $p < 0.005$ and 0.05, respectively). The same trend was observed in control PS1 animals but did not reach statistical significance (U's > 8, ns). At 24 months of age APP/PS1 mice still showed reduced brain and intracranial volumes in comparison with PS1 mice but this difference was no longer statistically significant ($U = 15$ and 14, respectively, ns)(Fig. 2A).

In a second step of analysis, MRI brain volumes were corrected for inter-individual variation of the intracranial volume (Fig. 2B) and were similar in young APP/PS1 and PS1 animals ($U = 21$, ns). Corrected brain volumes were not modified by age in PS1 animals ($U = 9$, ns) but strongly decreased in old APP/PS1 mice ($U = 0$, $p < 0.001$). The atrophy process in 24-month-old APP/PS1 mice was confirmed by their lower corrected brain volumes in comparison to aged PS1 animals ($U = 3$; $p < 0.01$).

Complementary analysis indicated that the index of global brain atrophy derived from total CSF volume (Fig. 2B) was similar in young APP/PS1 and PS1 animals ($U = 21$, ns). It was not modified by age in PS1 animals ($U = 10$, ns) but increased with aging in the APP/PS1 group ($U = 1$, $p < 0.005$).

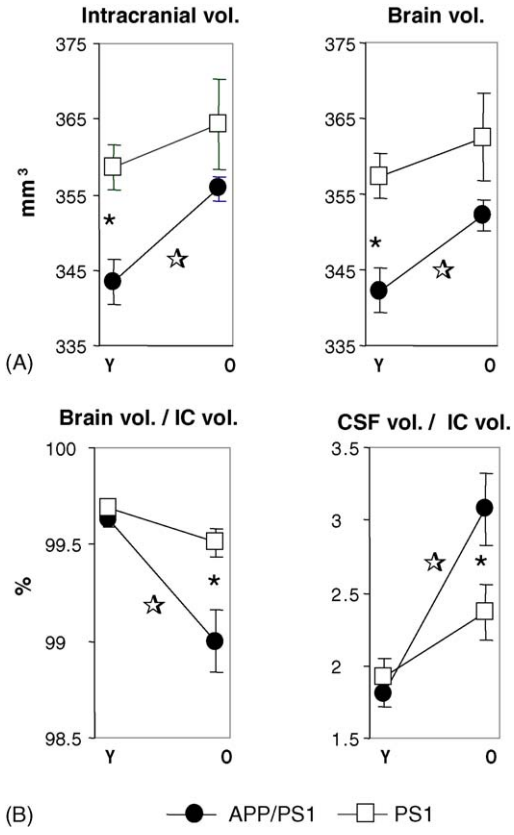

Fig. 2. (A) Comparison of intracranial and whole brain volumes measured by in vivo MRI in 10 weeks old (Y) and 24 months old (O) APP/PS1 and PS1 mice (mean ± S.E.M.). (B) Brain and CSF volume indices (i.e., after correction for individual differences in intracranial volume—IC). (☆) Age-related significant differences between animals of the same genotype; (*) significant differences between age-matched APP/PS1 and PS1 animals.

Accordingly, the index of global brain atrophy was significantly higher in 24-month-old APP/PS1 transgenics than in age-matched PS1 animals ($U=6$, $p<0.05$), thus confirming the brain atrophy in APP/PS1 mice.

3.2. Brain atrophy related to brain and body weights

Body and brain weights were similar in young APP/PS1 and PS1 animals (U's > 17, ns; Table 1). Both body and brain weights increased subsequently with aging in PS1 mice ($U=2$, $p<0.005$ and $U=8.5$, $p<0.05$, respectively) but not in APP/PS1 mice (U's > 17, ns). Therefore, reduced body and brain weights were observed in 24-month old APP/PS1 animals compared to age-matched PS1 mice (body weights: $U=3$; $p<0.001$; brain weights: $U=0$; $p<0.005$).

The brain weight/body weight ratio was comparable in young APP/PS1 and PS1 animals ($U=17$, ns; Table 1). However, while this ratio significantly decreased with aging in PS1 mice ($U=2$, $p<0.005$), it did not vary in APP/PS1 mice ($U=23$, ns). At 24 months of age the brain weight/body weight ratio was consequently lower in PS1 compared to APP/PS1 mice ($U=4$; $p<0.05$).

3.3. Measures of regional brain atrophies

3.3.1. Anterior brain areas

Total CSF volume in the anterior brain and the three indices of regional atrophy in the anterior brain (assessed from CSF volume of the lateral ventricles, third ventricle and peri-encephalic areas) were similar in young APP/PS1 and PS1 animals (U's > 17, ns) (Fig. 3A). Global and regional atrophy indexes were slightly but not significantly increased during aging in PS1 animals. On the contrary, aged APP/PS1, compared to young APP/PS1 mice, displayed a significant increase of global anterior brain atrophy index ($U=1$, $p<0.005$) and of regional atrophy indexes (third ventricle: $U=2$, $p<0.005$; pericortical areas: $U=4$, $p<0.01$). The differences between CSF indices from the anterior brain were however not significant when aged APP/PS1 were directly compared to age-matched PS1 mice (all U's > 8; ns). This suggested that the atrophy in anterior brain regions remained of limited importance.

Table 1
Mean ± S.E.M. of morphometric measures taken from APP/PS1 and PS1 animals

	Young		Old	
	PS1	APP/PS1	PS1	APP/PS1
Body weight (g)	20.3 ± 0.6	19.1 ± 0.5	31.4 ± 3.5 ↗	19.2 ± 1.3 ✸
Brain weight (mg)	495 ± 5	487 ± 6	520 ± 8 ↗	475 ± 9 ✸
Brain weight/body weight (%)	2.45 ± 0.06	2.55 ± 0.04	1.76 ± 0.16 ↙	2.52 ± 0.15 ✸
Brain length (mm)	9.0 ± 0.1	8.8 ± 0.1	9.0 ± 0.1	9.4 ± 0.1 ↗ ✸
Hippocampus volume/brain volume (%)[a]	7.8 ± 0.1	7.7 ± 0.2	9.4 ± 0.1 ↗	9.4 ± 0.3 ↗
Mammillary bodies surface (mm^2)	2.2 ± 0.2	2.3 ± 0.2	2.6 ± 0.2	2.1 ± 0.2
Midbrain height (mm)	2.64 ± 0.02	2.59 ± 0.03	2.83 ± 0.04 ↗	2.55 ± 0.03 ✸
Rostral corpus callosum thickness (mm)	0.44 ± 0.02	0.39 ± 0.02	0.49 ± 0.03	0.33 ± 0.03 ✸
Corpus callosum length (mm)	3.5 ± 0.2	3.4 ± 0.1	3.7 ± 0.1	3.5 ± 0.1
Mammillo-thalamic tract diameter (mm)	0.27 ± 0.02	0.26 ± 0.01	0.26 ± 0.01	0.26 ± 0.01

Significant differences between the two genotypes are highlighted. (↗↙) Significant increase/decrease between young and old mice of the same genotype (Aging effect); (✸) significant difference between PS1 and APP/PS1 mice at one particular age (Genotype effect).

[a] Histologically assessed hippocampal volumes were corrected by brain volumes also derived from postmortem brain sections.

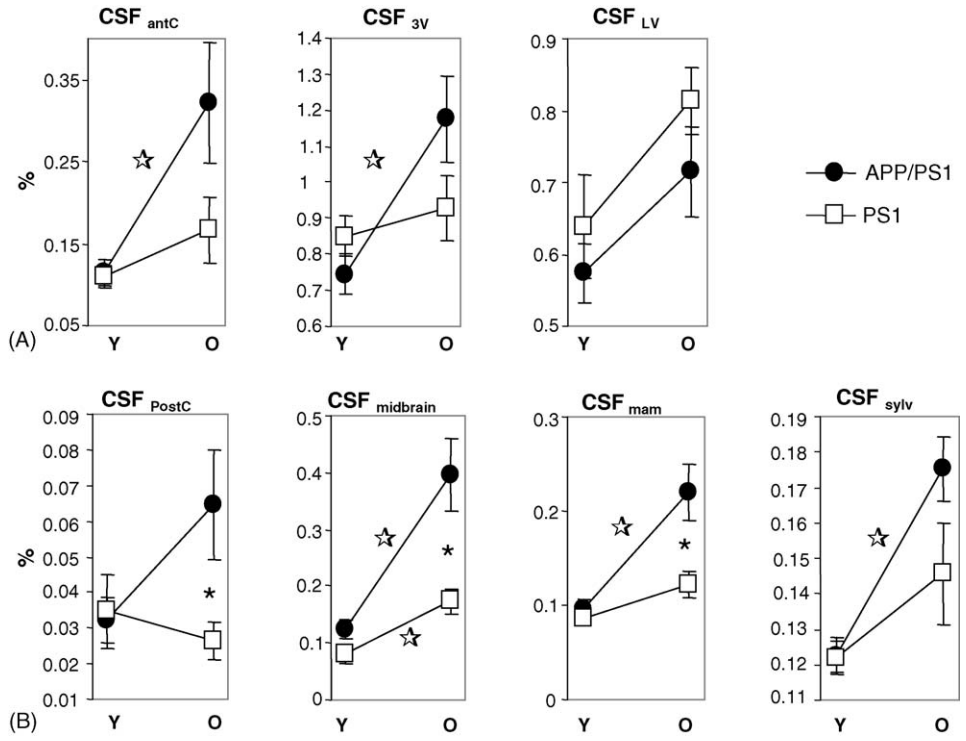

Fig. 3. Regional CSF volumes in young (Y) and old (O) PS1 and APP/PS1 genotypes (mean ± S.E.M.). (A) anterior peri-encephalic areas (CSF_{antC}), third ventricle and part of the lateral ventricle anterior to the interventricular foramen (CSF_{3V}), part of the lateral ventricles posterior to the interventricular foramen (CSF_{LV}). (B) Posterior peri-encephalic areas (CSF_{postC}), regions surrounding the midbrain ($CSF_{midbrain}$), mammillary fossa (CSF_{mam}) and aqueduct of Sylvius (CSF_{sylv}). (☆) Age-related significant differences between animals of the same genotype; (*) significant differences between age-matched APP/PS1 and PS1 animals.

3.3.2. Posterior brain areas

Index of CSF volume in the posterior part of the brain and the four indices of regional atrophy in the posterior brain (CSF volume of the mammillary fossa, areas surrounding the midbrain and aqueduct of Sylvius) were similar in young APP/PS1 and PS1 animals (U's > 14, ns) (Fig. 3B). Comparison of young and aged PS1 animals revealed an age-related significant increase of the midbrain CSF ($U = 3$, $p < 0.005$) but not of other indices (U's > 9, ns). On the other hand, comparison of young and aged APP/PS1 animals showed severe age-related increase of total posterior atrophy index ($U = 0$, $p < 0.001$) as well as regional indices related to the mammillary fossa ($U = 2$, $p < 0.005$), midbrain ($U = 0$, $p < 0.001$) and aqueduct of Sylvius ($U = 0$, $p < 0.001$). The CSF increase in pericortical posterior brain areas of APP/PS1 mice did not reach statistical significance ($U = 13$, ns). The severe atrophy of the posterior brain in aged APP/PS1 animals was also directly demonstrated by significant increases of CSF volumes in these mice compared to age-matched PS1 (posterior part of the brain: $U = 3$, $p < 0.01$; posterior peri-encephalic areas: $U = 6$, $p < 0.05$; mammillary fossa: $U = 5$, $p < 0.025$; areas surrounding the midbrain: $U = 1$, $p < 0.0025$). The only posterior brain region that did not demonstrate signs of atrophy in double transgenic mice was the Sylvius aqueduct area ($U = 11$; ns).

To specify the anatomical origin of the atrophy in the posterior brain, complementary morphological analyses were performed. The surface of the mammillary bodies, evaluated on histological slices, was similar in all the groups (U's > 9; ns). MRI- and histologically-based evaluation of the midbrain height and width were highly correlated ($r = 0.629$, $p < 0.0001$) and showed no differences between young APP/PS1 and PS1 animals (all U's > 15.5, ns). Size of the midbrain did not change significantly with age in APP/PS1 mice (U's > 15, ns) but largely increased in PS1 animals ($U = 0$, $p < 0.001$ and $U = 1.5$, $p < 0.005$, respectively for height and width measurements). Consequently, a significant reduction of the midbrain size was noted in aged APP/PS1 compared to aged PS1 animals ($U = 0$, $p < 0.0025$ for MR evaluation and $U = 0.5$, $p < 0.0025$ for histological measure)(Fig. 4A).

3.3.3. Hippocampus

The histologically-assessed hippocampal volumes (absolute and corrected by brain volume) were very similar in the two genotypes for animals evaluated at the same age (comparison between PS1 and APP/PS1 mice, at 10 weeks: $U = 24$, ns; at 24 months: $U = 10$, ns) (Fig. 5). For both genotypes, a significant increase of hippocampal (non-corrected and corrected) volume was found when aged animals were compared to young ones (all U's = 0; p's < 0.005 for PS1 animals and p's < 0.001 for APP/PS1 animals). Brain and hippocampal volumes were correlated in young mice, in both genotypes (PS1: $r = 0.819$, $p < 0.025$; APP/PS1: $r = 0.89$, $p < 0.01$). At 24

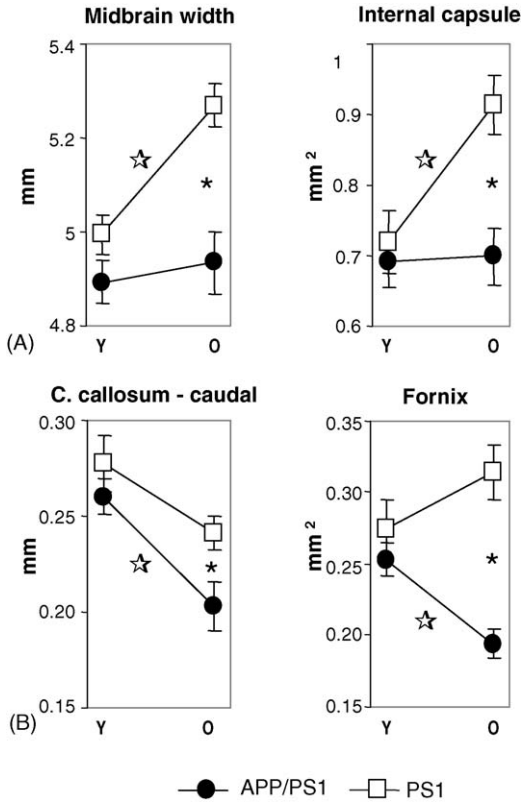

Fig. 4. Evaluation of the size of various brain structures in 10 weeks old (Y) and 24 months old (O) APP/PS1 and PS1 mice (mean ± S.E.M.). (A) midbrain and internal capsule showed growth arrest in APP/PS1 transgenics. (B) Caudal part of the corpus callosum and fornix demonstrated shrinkage during aging in APP/PS1 mice. (☆) Age-related significant differences between animals of the same genotype; (*) significant differences between age-matched APP/PS1 and PS1 animals.

months of age, however, this correlation was only observed in PS1 animals ($r = 0.91$, $p < 0.025$) but not anymore in APP/PS1 mice ($r = -0.1$, ns).

3.3.4. Fiber tracts

(1) The corpus callosum was easily discernable in all animals. No sign of callosal agenesis was detected in any of the 28 studied mice. Rostral and caudal corpus callosum thickness were correlated ($r = 0.378$; $p < 0.05$) and did not differ in young APP/PS1 and PS1 animals (U's > 11, ns; see Table 1 and Fig. 4B). During aging, PS1 animals did not display significant variations of callosal size (all U's > 10; ns). On the contrary, aged APP/PS1 showed a reduced thickness of the caudal corpus callosum ($U = 1.5$, $p < 0.005$) in comparison to young APP/PS1 animals (Fig. 4). The rostral thickness of the corpus callosum was not affected in this genotype ($U = 14$, ns). Atrophy of the corpus callosum was directly confirmed by comparing aged APP/PS1 mice with age-matched PS1 mice (rostral thickness: $U = 3$, $p < 0.01$, and caudal thickness: $U = 5$, $p < 0.025$). Finally, the corpus callosum length was not different in the four groups of animals (U's > 10.5, ns).

(2) The fornix diameter was similar in young APP/PS1 and PS1 animals ($U = 21.5$, ns). It decreased with age in APP/PS1 animals ($U = 3.5$, $p < 0.005$) but not in PS1 mice ($U = 15$, ns). Therefore, in old mice the fornix diameter was reduced in APP/PS1 animals as compared to PS1 ($U = 0$, $p < 0.005$; see Figs. 4B and 6).

(3) The internal capsule surface was similar in young APP/PS1 and PS1 animals ($U = 25$, ns). Its size increased with age in PS1 animals ($U = 6$, $p < 0.05$) but not in APP/PS1 ($U = 16$, ns). This led to a significant higher

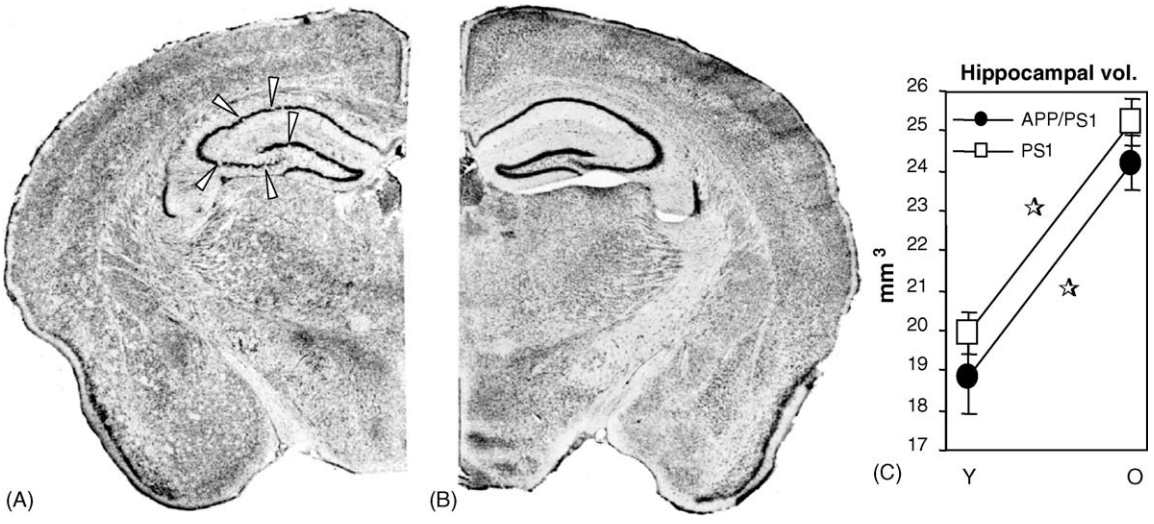

Fig. 5. Hippocampal gross morphology in 24 months old APP/PS1 (A) and PS1 (B) mice. The graph (C) shows the size of the hippocampus in young (Y) and old (O) mice. Hippocampal growth occurred in both genotypes. Despite severe plaque-induced alterations of cytoarchitectony (arrow heads in A), the hippocampus of aged APP/PS1 mice was not significantly atrophied compared with PS1 control animals. (☆) Age-related significant differences between animals of the same genotype.

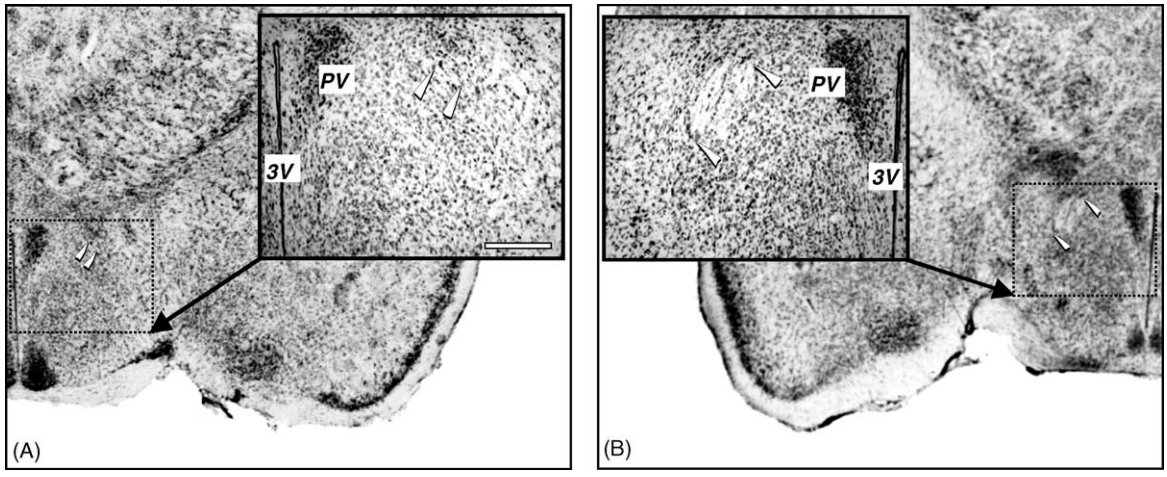

Fig. 6. Morphological analysis revealed a reduction in fornical cross-sectional diameter in old double APP/PS1 transgenics (A) compared with age-matched PS1 mice (B). Insets in upper corners represent high magnification of the area bordered with dotted lines in the background photographs. Arrow heads set the limits of the fornix diameter. Scale bar, for both insets: 300 μm. Annotations: PV, paraventricular hypothalamic nucleus; 3V, third ventricle.

surface area of the capsule in aged PS1 animals than in APP/PS1 mice ($U = 1$, $p < 0.01$)(Fig. 4A).

(4) The diameter of the mammillothalamic tract did not significantly vary between the two genotypes and between ages (all U's > 17, ns).

3.4. Cerebral Aβ deposition: quantification and correlates

Amyloid deposition was very extensive in aged APP/PS1 mice (see Fig. 1F). Congo red stained plaques were mainly observed in iso- and archicortical (hippocampus) brain areas as well as in selected subcortical regions (e.g., thalamus, septal nuclei, amygdala, accumbens nucleus) as previously depicted [2]. PS1 animals did not show any amyloid deposits as expected. Statistical analyses indicated that the amyloid load of APP/PS1 animals (proportion of surface occupied by Congo red stained material) was not correlated with any of the more than thirty in vivo or postmortem variables in brain morphology that we evaluated.

4. Discussion

4.1. Cerebral atrophy in APP/PS1 transgenic mice

The aim of the present study was to assess the impact of cerebral amyloidosis on gross brain morphology in transgenic mice overexpressing Alzheimer-associated mutated genes. We therefore evaluated the occurrence of cerebral atrophy (1) in young adults (10-week-old) transgenic APP/PS1 mice that did not show cerebral Aβ plaques, and (2) in 24 months old APP/PS1 animals demonstrating massive cerebral amyloidosis. Age-matched amyloid deposit-free PS1 animals were used as controls.

At young ages APP/PS1 mice showed reduced brain and intracranial volumes compared with PS1 animals. Then, during adulthood, the double transgenics demonstrated both growth of the brain and of the head. At 24 months of age APP/PS1 mice still maintained a trend towards lower brain and cranial sizes compared with aged-matched control mice, but differences between genotypes were no longer significant. This suggests that the time window for head–brain development/growth in double transgenics shifts or, at least, is modified compared with normal mice.

Direct analysis of brain and CSF volumes was then performed by correcting MRI volume data by intracranial size in order to take into account inter-individual variations in head size. With such ponderated computations, no significant differences were detected between young APP/PS1 and PS1, regardless of the measures considered (total or regional volumes). This indicates that, despite differences in raw volumes, the two studied genotypes showed similar proportional sizes of skull and brain. On the other hand, a significant reduction of brain size and a concomitant increase of CSF volume was found in aged APP/PS1 mice compared with age-matched PS1 as well as young APP/PS1 mice. To our knowledge, this is the first demonstration of global brain atrophy in transgenic mice modeling AD.

Evaluation of the atrophy process by the bias of CSF volumes revealed a discrete atrophy process in the anterior brain of APP/PS1 transgenics. It was only evidenced by an increase in CSF volume during aging that was statistically significant in double transgenics (but not in PS1 mice). Concurrently a robust, although unexpected, dilation of the posterior CSF space was noted in 24 months APP/PS1 animals compared with old PS1 as well as young APP/PS1 mice. The subsequent step of our investigations was to identify the anatomical loci responsible for the increased CSF volumes in posterior cerebral regions. Reduced volume of the caudal brain was not

related to mammillary bodies because, as shown by histology, size of this structure was unaffected by the genotype and did not vary with age. Posterior atrophy was more readily linked to the midbrain region as both MRI and histological analyses revealed a smaller size of the mesencephalic area in aged APP/PS1 than in age-matched PS1 animals.

As a striking result we did not find any evidence of hippocampal atrophy, even in 2 years old APP/PS1 transgenics. These histological findings were indirectly corroborated, from MRI, by the absence of dilation of the part of the lateral ventricles that surrounds the dorsal hippocampus.

Evaluation of fiber tracts revealed a complex pattern of morphological alterations in APP/PS1 mice: while the mammillo-thalamic tract size was not modified by the genotype, a reduction of the thickness of the corpus callosum and of the surface of the fornix and internal capsule were detected in aged APP/PS1 compared with PS1 mice.

4.2. Brain atrophy versus growth arrest

During adulthood and subsequent aging, morphological abnormalities occurring in double transgenics were related to two different processes. First, our results showed that in control mice some brain structures (midbrain, hippocampus, internal capsule) had continuous growth throughout adulthood. This phenomenon has been addressed and documented in previous studies (e.g., hippocampal growth [29,32]). Similar local brain growth was noted in APP/PS1 animals at the level of the hippocampus. However, other structures (midbrain and the internal capsule) maintained a constant size across age in APP/PS1 mice. This underlines that brain volume reductions noted in aged APP/PS1 transgenics compared to old PS1 mice can readily be due to an interrupted growth of selected cerebral areas rather than to tissue shrinkage arising with aging. A second process that could be termed as "classical atrophy" concomitantly occurred in APP/PS1 mice. Hence, for some brain regions (such as the fornix and the caudal corpus callosum), a clear loss of tissue was evidenced during aging in aged double transgenics. This led to reduced brain structure sizes in aged APP/PS1 compared to aged PS1 mice that did not show similar age-related morphological alterations.

Therefore, these data suggest that global brain volume reduction and concomitant CSF increase observed in 24-month-old APP/PS1 mice is finally due to a dual process, involving both interruption of continuous (normal) brain growth on one side and tissue loss/shrinkage on the other side.

4.3. Comparison with AD-related brain atrophy and other transgenic mouse models

Global brain atrophy is constantly reported following neuropathological examination of AD patients [43]. A few studies have addressed the question of cerebral atrophy in genetically modified mice modeling AD. To our knowledge all these studies were performed on the PDAPP monogenic model and did not describe significant global brain atrophy [14,32,45]. In our study, when inter-individual differences for skull size were taken into account, a global CSF increase and a concomitant reduction of brain volume could be detected in APP/PS1 animals. A superficial analysis of this point may indicate that the transgenic APP/PS1 model mimics the atrophy associated with AD. However, systematic evaluation of regional CSF volumes suggested that atrophy processes involved mainly posterior brain areas, a pattern very different than that reported in AD. Moreover, our observations indicate that the CSF volume increase in posterior areas is at least partly related to the smaller size of the midbrain in aged APP/PS1 compared to PS1 mice. In humans, atrophy of the midbrain is reported during the course of aging [13,35], but, to our knowledge, is not potentiated in AD patients.

Atrophy of the *hippocampal* formation is a major hallmark of AD [22]. In the PDAPP model, a severe loss of hippocampal volume is also invariably reported, even without precise quantification [11,14,32,45]. It is, however, characterized by a very early and dramatic onset [14,32] which differs strikingly from the progressive hippocampal volume loss noted during the course of AD [18]. It has thus been suggested that hippocampal atrophy in PDAPP mice is related to a neurodevelopmental abnormality, possibly linked to parenchymal accumulation of soluble Aβ, rather than to a degenerative process [11,32]. Our model did not display developmental related atrophy of the hippocampus because the size of the hippocampus was similar in the two genotypes. Moreover, during adulthood, the hippocampus grew in a similar way in APP/PS1 and in PS1 and the size of the hippocampus that we measured in 24 months APP/PS1 and PS1 animals was comparable to that reported in the literature for aged wild type mice [44]. It can thus not be argued that our control PS1 animals were also atrophied. The absence of hippocampal atrophy in our model might concurrently be related to some already-demonstrated protective effect of the PS1 transgene [26] but, in our opinion, could be better explained by variables affecting the phenotype of the different studied models [19]. Such variables can be found at the level of mutated transgenes, promoters or genetic background used to establish the transgenic lines. In any case, the absence of hippocampal atrophy in our APP/PS1 model that, otherwise, displayed very aggressive amyloid pathology suggests that hippocampal tissue loss, as observed in the PDAPP mouse model and in human pathology, is not invariably associated with extracellular Aβ deposition (see next section).

The reduction in size of the internal capsule we have reported in the present study has not been described in either AD patients [4] or transgenic mice models although a recent study has demonstrated morphological abnormalities at the level of the cerebral peduncles in aged PDAPP mice [37], an observation fitting well with our findings.

Normal development followed by age-related shrinkage of fiber tracts, such as the *corpus callosum or the fornix*, was another finding from our study. Corpus callosum [41,42]

as well as fornical [6] atrophies are both reported in AD patients. They are also described in PDAPP mice in studies using histological, anatomical MRI or diffusion tensor imaging approaches [14,32,37]. In the PDAPP transgenic model the corpus callosum atrophy is however spectacular, varying from large reduction in size to complete agenesis [11,14,32]. It is far more severe than the atrophy described in our study and in AD pathology [41,42]. Noticeably, in PDAPP mice, the atrophy of the corpus callosum and of the fornix is described at relative young ages (3 months) suggesting that it is also related to some neurodevelopmental disorders. The pattern of atrophy in our model is therefore different because the atrophy was not related to developmental alterations as suggested by similar size in young adult animals.

Because the fornix is a major afferent/efferent pathway of the hippocampus and because it is atrophied in PDAPP mice and AD patients that both display hippocampal atrophy, it might be tempting to directly associate atrophy of the fornix with hippocampal volume loss. Nevertheless, we reported here fornical atrophy in APP/PS1 mice in the absence of atrophy in the hippocampus or mammillary bodies. This suggests that atrophy of the fornix may be linked to fiber tract alterations independent of anterograde/retrograde neurodegenerative processes and involves selective brain pathways (e.g., corpus callosum and fornix) but spares others (e.g., mammillo-thalamic tract).

4.4. Cerebral amyloidosis and other neurobiological basis for brain atrophy

Several observations in humans indicate that the accumulation of neurofibrillary tangles is crucially involved in the atrophy process [3,25]. A somewhat weak correlation between brain atrophy and amyloid load has also been reported in AD and in old mammals developing Aβ deposits [25,40], suggesting that amyloid is an additional causal factor.

Our study reports the absence of hippocampal atrophy in aged APP/PS1 animals despite heavy amyloid burden and, more importantly, showed that all the (nearly 30) histological or MRI-based morphological measures taken to quantify global and local atrophies were not correlated with amyloid load. This suggests that extracellular Aβ deposits were not directly involved in the genesis of cerebral atrophy. Recent data suggest that intracellular aggregated Aβ is more efficient than parenchymal amyloid plaques to promote hippocampal neuronal loss (and presumably associated local atrophies) [7]. While supporting the hypothesis of a pathogenic role for Aβ, these latter observations strengthen the contention that extracellular plaques do not play a key role per se in macroscopic brain morphological alterations.

The CSF increase in posterior brain regions was (at least partly) related to the reduced size of the midbrain region in APP/PS1 animals. In this area, the plaque density was very low in comparison to isocortical and hippocampal areas. This also underlines the apparent independence of Aβ deposition and onset of localized atrophies.

Our results obtained in mice that did not display tangles, thus support the hypothesis that, in humans, AD-related cortical and hippocampal atrophy is mainly associated with neurofibrillary lesions rather than with Aβ deposition. The corollary is that the lack of NFT lesions in the APP/PS1 animals may explain the different atrophy pattern in these mice compared with AD subjects.

The origin of fiber tract atrophy, in the absence of obvious afferent/efferent brain structure atrophies remains to be elucidated. Because fiber tract alterations are found in different transgenic lines (PDAPP and present APP/PS1 model), one may hypothesize that they are directly related to the expression of the mutated APP transgene. APP is known to play a key role in neurite outgrowth and axonal guidance during development [31,36] and it has been recently demonstrated that manipulations of APP and APP-like proteins genes, including underexpression and even knocking-out, are accompanied by altered brain development [16] and in particular by dramatic changes at the level of forebrain commissures [23]. Therefore, one cannot rule out the possibility that overexpressing (human) APP, especially under mutated forms, leads to detrimental effects during the development of brain connections. Previous studies reported that the degree of fiber tract alteration after modification of the APP gene is also related to animal's genetic background [23]. This may explain the different patterns and intensities of fiber tracts alterations in the PDAPP and APP/PS1 models. The mechanism underlying the origin of fiber tract atrophy might concurrently be explained by (1) a reduced population of existing fibers, such as callosal axons that project from one hemisphere to the other and appear to malfunction in APP transgenics [38]. (2) A reduced number or loss of function of oligodendrocytes responsible for axon myelination. Indeed, recent studies suggest that oligodendrocytes are vulnerable to Aβ toxicity [27]. Deciphering the exact nature of fiber tract atrophies will be the focus of subsequent research efforts.

4.5. Concluding remarks

To summarize, in an APP/PS1 transgenic mouse model, we have provided evidence of slight age-related CSF volume increase in anterior brain areas and of a more severe CSF increase in posterior brain areas. The latter was related to the lack of development of the midbrain during the adulthood period. We also reported alteration of some but not all fiber tracts, that might be related to either interrupted growth or age-related shrinkage in adult APP/PS1. The pathogenic events leading to such morphological alterations however remain to be elucidated.

Selected localized brain atrophy in APP/PS1 mice, associated with the absence of severe cortical and hippocampal decline, indicate a pattern of gross anatomical alteration somehow different than those reported in AD patients. This suggests that overexpression of mutated APP

is not invariably accompanied by AD-like brain atrophy. Moreover, we present direct evidence that the severity of atrophy was not reliably correlated with the amyloid load. This challenged the opportunity for using in vivo atrophy detection as a surrogate biomarker for extracellular Aβ accumulation. Recent approaches using MRI with targeted contrast agents [48] or multiphoton microscopy [21] might be more suitable for addressing such objectives.

Conflict of interest

Transgenic mice used in the present study were a generous gift from Sanofi-Aventis to Marc Dhenain who did not receive any additional financial support from the company. Benoît Delatour has received funding from Sanofi-Aventis but to carry out experimental studies different from the ones described in the present paper.

Acknowledgments

The Sanofi-Aventis Alzheimer network is greatly acknowledged for providing transgenic animals used in this study. This study was supported by the CNRS-INSERM joint program 'Small Animal Imaging' (SUB-05/DR12/2002), the INSERM program 'United Thematic Actions on Aging', the Del Duca Foundation, the 'Federation for Brain Research' program and the 'Neuroscience ACI research' program from the French Minister for Research. We are grateful to Dr. S. Davis and J. Horwood for carefully reading and correcting the manuscript.

References

[1] Ashe KH. Learning and memory in transgenic mice modeling Alzheimer's disease. Learn Mem 2001;8(6):301–8.
[2] Blanchard V, Moussaoui S, Czech C, Touchet N, Bonici B, Planche M, et al. Time sequence of maturation of dystrophic neurites associated with Ab deposits in APP/PS1 transgenic mice. Exp Neurol 2003;184(1):247–63.
[3] Bobinski M, Wegiel J, Wisniewski HM, Tarnawski M, Reisberg B, De Leon MJ, et al. Neurofibrillary pathology-correlation with hippocampal formation atrophy in Alzheimer disease. Neurobiol Aging 1996;17(6):909–19.
[4] Bozzali M, Falini A, Franceschi M, Cercignani M, Zuffi M, Scotti G, et al. White matter damage in Alzheimer's disease assessed in vivo using diffusion tensor magnetic resonance imaging. J Neurol Neurosurg Psychiatry 2002;72(6):742–6.
[5] Braak H, Braak E. Staging of Alzheimer's disease-related neurofibrillary changes. Neurobiol Aging 1995;16(3):271–8 [Discussion 8-84].
[6] Callen DJ, Black SE, Gao F, Caldwell CB, Szalai JP. Beyond the hippocampus: MRI volumetry confirms widespread limbic atrophy in AD. Neurology 2001;57(9):1669–74.
[7] Casas C, Sergeant N, Itier JM, Blanchard V, Wirths O, van der Kolk N, et al. Massive CA1/2 neuronal loss with intraneuronal and N-terminal truncated Abeta42 accumulation in a novel Alzheimer transgenic model. Am J Pathol 2004;165(4):1289–300.
[8] Delesse MA. Procédé mécanique pour déterminer la composition des roches. C R Acad Sci 1847;25:544–55.
[9] Dhenain M, Chenu E, Hisley CK, Aujard F, Volk A. Regional atrophy in the brain of lissencephalic mouse lemur primates: measurement by automatic histogram-based segmentation of MR images. Magnet Reson Med 2003;50:984–92.
[10] Dhenain M, Michot JL, Privat N, Picq JL, Boller F, Duyckaerts C, et al. MRI description of cerebral atrophy in mouse lemur primates. Neurobiol Aging 2000;21(1):81–8.
[11] Dodart JC, Mathis C, Saura J, Bales KR, Paul SM, Ungerer A. Neuroanatomical abnormalities in behaviorally characterized APP(V717F) transgenic mice. Neurobiol Dis 2000;7(2):71–85.
[12] Dominguez DI, De Strooper B. Novel therapeutic strategies provide the real test for the amyloid hypothesis of Alzheimer's disease. Trends Pharmacol Sci 2002;23(7):324–30.
[13] Doraiswamy PM, Na C, Husain MM, Figiel GS, McDonald WM, Ellinwood Jr EH, et al. Morphometric changes of the human midbrain with normal aging: MR and stereologic findings. AJNR Am J Neuroradiol 1992;13(1):383–6.
[14] Gonzalez-Lima F, Berndt JD, Valla JE, Games D, Reiman EM. Reduced corpus callosum, fornix and hippocampus in PDAPP transgenic mouse model of Alzheimer's disease. Neuroreport 2001;12(11):2375–9.
[15] Hardy JA, Higgins GA. Alzheimer's disease: the amyloid cascade hypothesis. Science 1992;256(5054):184–5.
[16] Herms J, Anliker B, Heber S, Ring S, Fuhrmann M, Kretzschmar H, et al. Cortical dysplasia resembling human type 2 lissencephaly in mice lacking all three APP family members. EMBO J 2004;23(20):4106–15.
[17] Higgins GA, Jacobsen H. Transgenic mouse models of Alzheimer's disease: phenotype and application. Behav Pharmacol 2003;14(5–6):419–38.
[18] Jack Jr CR, Dickson DW, Parisi JE, Xu YC, Cha RH, O'Brien PC, et al. Antemortem MRI findings correlate with hippocampal neuropathology in typical aging and dementia. Neurology 2002;58(5):750–7.
[19] Janus C, Westaway D. Transgenic mouse models of Alzheimer's disease. Physiol Behav 2001;73(5):873–86.
[20] Jellinger KA, Bancher C. Neuropathology of Alzheimer's disease: a critical update. J Neural Transm Suppl 1998;54:77–95.
[21] Klunk WE, Bacskai BJ, Mathis CA, Kajdasz ST, McLellan ME, Frosch MP, et al. Imaging Abeta plaques in living transgenic mice with multiphoton microscopy and methoxy-X04, a systemically administered Congo red derivative. J Neuropathol Exp Neurol 2002;61(9):797–805.
[22] Lehericy S, Baulac M, Chiras J, Pierot L, Martin N, Pillon B, et al. Amygdalohippocampal MR volume measurements in the early stages of Alzheimer disease. AJNR: Am J Neuroradiol 1994;15(5):929–37.
[23] Magara F, Muller U, Li ZW, Lipp HP, Weissmann C, Stagljar M, et al. Genetic background changes the pattern of forebrain commissure defects in transgenic mice underexpressing the beta-amyloid-precursor protein. Proc Natl Acad Sci USA 1999;96(8):4656–61.
[24] Nagy Z, Hindley NJ, Braak H, Braak E, Yilmazer-Hanke DM, Schultz C, et al. The progression of Alzheimer's disease from limbic regions to the neocortex: clinical, radiological and pathological relationships. Dement Geriatr Cogn Disord 1999;10(2):115–20.
[25] Nagy Z, Jobst KA, Esiri MM, Morris JH, King EM, MacDonald B, et al. Hippocampal pathology reflects memory deficit and brain imaging measurements in Alzheimer's disease: clinicopathologic correlations using three sets of pathologic diagnostic criteria. Dementia 1996;7(2):76–81.
[26] Nakajima M, Miura M, Aosaki T, Shirasawa T. Deficiency of presenilin-1 increases calcium-dependent vulnerability of neurons to oxidative stress in vitro. J Neurochem 2001;78(4):807–14.
[27] Pak K, Chan SL, Mattson MP. Presenilin-1 mutation sensitizes oligodendrocytes to glutamate and amyloid toxicities, and exacerbates white matter damage and memory impairment in mice. Neuromol Med 2003;3(1):53–64.

[28] Paxinos G, Franklin KBJ. The mouse brain in stereotaxic coordinates. 2nd ed. San Diego: Academic Press; 2001.
[29] Peirce JL, Chesler EJ, Williams RW, Lu L. Genetic architecture of the mouse hippocampus: identification of gene loci with selective regional effects. Genes Brain Behav 2003;2(4):238–52.
[30] Puchtler H, Sweat F, Levine M. On the binding of Congo red by amyloid. J Histochem Cytochem 1962;10:355–64.
[31] Qiu WQ, Ferreira A, Miller C, Koo EH, Selkoe DJ. Cell-surface beta-amyloid precursor protein stimulates neurite outgrowth of hippocampal neurons in an isoform-dependent manner. J Neurosci 1995;15(3 Pt. 2):2157–67.
[32] Redwine JM, Kosofsky B, Jacobs RE, Games D, Reilly JF, Morrison JH, et al. Dentate gyrus volume is reduced before onset of plaque formation in PDAPP mice: a magnetic resonance microscopy and stereologic analysis. Proc Natl Acad Sci USA 2003;100(3):1381–6.
[33] Rosen GD, Harry JD. Brain volume estimation from serial section measurements: a comparison of methodologies. J Neurosci Methods 1990;35(2):115–24.
[34] Schmitz C, Rutten BP, Pielen A, Schafer S, Wirths O, Tremp G, et al. Hippocampal neuron loss exceeds amyloid plaque load in a transgenic mouse model of Alzheimer's disease. Am J Pathol 2004;164(4):1495–502.
[35] Shah SA, Doraiswamy PM, Husain MM, Figiel GS, Boyko OB, McDonald WM, et al. Assessment of posterior fossa structures with midsagittal MRI: the effects of age. Neurobiol Aging 1991; 12(4):371–4.
[36] Small DH, Clarris HL, Williamson TG, Reed G, Key B, Mok SS, et al. Neurite-outgrowth regulating functions of the amyloid protein precursor of Alzheimer's disease. J Alzheimers Dis 1999;1(45):275–85.
[37] Song SK, Kim JH, Lin SJ, Brendza RP, Holtzman DM. Diffusion tensor imaging detects age-dependent white matter changes in a transgenic mouse model with amyloid deposition. Neurobiol Dis 2004;15(3):640–7.
[38] Stern EA, Bacskai BJ, Hickey GA, Attenello FJ, Lombardo JA, Hyman BT. Cortical synaptic integration in vivo is disrupted by amyloid-beta plaques. J Neurosci 2004;24(19):4535–40.
[39] Takeuchi A, Irizarry MC, Duff K, Saido TC, Hsiao Ashe K, Hasegawa M, et al. Age-related amyloid beta deposition in transgenic mice overexpressing both Alzheimer mutant presenilin 1 and amyloid beta precursor protein Swedish mutant is not associated with global neuronal loss. Am J Pathol 2000;157(1):331–9.
[40] Tapp PD, Siwak CT, Gao FQ, Chiou JY, Black SE, Head E, et al. Frontal lobe volume, function, and beta-amyloid pathology in a canine model of aging. J Neurosci 2004;24(38):8205–13.
[41] Teipel SJ, Bayer W, Alexander GE, Zebuhr Y, Teichberg D, Kulic L, et al. Progression of corpus callosum atrophy in Alzheimer disease. Arch Neurol 2002;59(2):243–8.
[42] Teipel SJ, Hampel H, Pietrini P, Alexander GE, Horwitz B, Daley E, et al. Region-specific corpus callosum atrophy correlates with the regional pattern of cortical glucose metabolism in Alzheimer disease. Arch Neurol 1999;56(4):467–73.
[43] Valk J, Barkhof F, Scheltens P. Magnetic resonance in dementia. Heidelberg, Berlin, New York: Springer-Verlag; 2002. p. 353.
[44] Von Bohlen und Halbach O, Unsicker K. Morphological alterations in the amygdala and hippocampus of mice during ageing. Eur J Neurosci 2002;16(12):2434–40.
[45] Weiss C, Venkatasubramanian PN, Aguado AS, Power JM, Tom BC, Li L, et al. Impaired eyeblink conditioning and decreased hippocampal volume in PDAPP V717F mice. Neurobiol Dis 2002;11(3):425–33.
[46] Wirths O, Multhaup G, Czech C, Blanchard V, Moussaoui S, Tremp G, et al. Intraneuronal Abeta accumulation precedes plaque formation in beta-amyloid precursor protein and presenilin-1 double-transgenic mice. Neurosci Lett 2001;306(1–2):116–20.
[47] Wirths O, Multhaup G, Czech C, Blanchard V, Tremp G, Pradier L, et al. Reelin in plaques of beta-amyloid precursor protein and presenilin-1 double-transgenic mice. Neurosci Lett 2001; 316(3):145–8.
[48] Zaim Wadghiri Y, Sigurdsson EM, Sadowski M, Elliott JI, Li Y, Scholtzova H, et al. Detection of Alzheimer's amyloid in transgenic mice using magnetic resonance microimaging. Magnet Reson Med 2003;50:293–302.